Improvement of properties in Cu–Ag composites by doping induced microstructural refinement

Congcong Zhao [a,b], Rongmei Niu [c], Yan Xin [c], Daniel Brown [c], David McGuire [c], Engang Wang [a,d,**], Ke Han [c,*]

[a] *Key Laboratory of Electromagnetic Processing of Materials (Ministry of Education), Northeastern University, Shenyang, Liaoning, 110819, China*
[b] *Jihua Laboratory, Foshan, Guangdong, 528000, China*
[c] *National High Magnetic Field Laboratory, Florida State University, Tallahassee, 32310, FL, USA*
[d] *School of Metallurgy, Northeastern University, Shenyang, Liaoning, 110819, China*

ABSTRACT

The microstructure, precipitation kinetics, electrical conductivity, and mechanical properties of Cu-7.9 wt%Ag and Cu-5.8 wt%Ag doped with 0.6 wt%Nb were investigated. As-cast microstructure revealed both discontinuous and continuous precipitation of Ag in Cu matrix. Differential scanning calorimetry data indicated that continuous precipitation occurred at higher temperatures with higher activation energy. Both micro-sized and nano-sized Nb particles were observed in the Nb-doped Cu–Ag alloy. The doping of Nb significantly suppressed the growth of discontinuous Ag precipitates and consequently increased the activation energy and the volume fraction of continuous Ag precipitates. Because of larger volume fraction of finer-spaced continuous Ag precipitates, the Nb-doped alloy showed higher hardness and strength than the un-doped Cu–Ag. After cold-rolling, the strength of the Nb-doped alloy remained higher than that of the un-doped Cu–Ag.

1. Introduction

High-field magnets are powerful tools for research in such fields as materials science, chemistry, physics, and biology [1]. These magnets require conductors with both high strength and high electrical conductivity. High strength is required for resisting Lorentz forces, and high electrical conductivity for reducing Joule heat.

Cu–Nb composite is a candidate for high-field magnet conductors [2–13]. In this composite, primary Nb dendrites that are formed during the casting become curled ribbons after severe plastic deformation. Nb has negligible solubility in Cu matrix, so it does not significantly decrease the electrical conductivity of Cu [14]. Previous work has indicated that Cu–Nb composites achieve strength of 1000 MPa when strain values reach about 8 [2]. Cu-20 wt%Nb has reached an ultimate tensile strength (UTS) up to 2.2 GPa at deformation strain of 12 [12,13]. Because of its high melting point, however, Cu–Nb is difficult to cast. Thus, researchers have instead used accumulative drawing and bundling or accumulative roll bonding to make filament or multilayered Cu–Nb nano-composites [15–17]. These approaches, however, require very large deformation strain (≥ 6), which makes the fabrication of large size conductors difficult and expensive.

Compared to Cu–Nb, Cu–Ag composites can be cast at lower temperature and fabricated under smaller deformation strain [18–31]. Researchers who have studied composition and microstructure in Cu–Ag, however, have found that, when they increased Ag to 72 wt%, the strength of the composite increased gradually, but electrical conductivity decreased substantially [22]. In order to maintain high conductivity, researchers kept Ag content at 24 wt% or lower, which allowed them to achieve UTS of 1 GPa and electrical conductivity of 80% International Annealed Copper Standard (IACS) in wire fabricated at a deformation strain of 4.6 (i.e. reduction-in-area of 99%) [22]. For comparison, a conductor with 100% IACS would have electrical resistivity of 1.7241 mV cm.

To increase conductivity and reduce the proportion of precious metal, researchers explored Cu–Ag composites that had even lower Ag content. The strength developed in these composites was attributed to work hardening, precipitation strengthening, solid-solution strengthening, and grain boundary strengthening [26,32]. Among those factors,

precipitation strengthening from Ag was the most important strengthening mechanism. Although solubility limitations at eutectic temperature (779.1 °C) were as high as 8.8 wt% for Cu in Ag and 7.5 wt% for Ag in Cu, solubility was lower than 0.06 wt% at room temperature [33]. This provides a driving force to precipitate Ag out of supersaturated Cu matrix by a precipitation reaction with decreasing temperature. Researchers found both discontinuous precipitation (DP) and continuous precipitation (CP) of Ag, depending not only on Ag content in the composite but also on the temperature of heat treatment [33–39]. They found that the volume fraction of DP, which is often partially suppressed by high Ag content, was apparently raised by heat treatment even at low temperatures [39]. In composites with Ag content as low as 8 wt%, however, CP volume fraction was strongly favored by heat treatment at high temperature [40].

Both wire drawing [41–43] and rolling [7,24] have been found to form a filamentary microstructure in Cu–Ag composites by aligning Ag precipitates parallel to the deformation orientation. The size and distribution of Ag precipitates in the initial state before deformation play an important role in controlling strength and electrical conductivity in the finished products. Strength varies with the percentage of Ag in the composites. To further improve strength, research is needed to understand the contributions made by precipitates (both DPs and CPs) under various conditions.

To improve properties and reduce production cost, researchers have added certain third elements into the Cu–Ag alloy. They found that, because of reduced Ag diffusion rates along grain boundaries, the addition of more than 0.05 wt% Zr favored the formation of CPs in Cu matrix by suppressing the formation of DPs. After deformation at drawing strain up to 5.8, interspersed with heat treatment, tensile strength and electrical conductivity reached 1.4 GPa and 60%IACS, respectively, in Cu-7wt%Ag-0.05 wt%Zr [36,44–50]. Because of extensive research on Cu–Nb and Cu–Ag binary systems, Nb was chosen as another third-element [51–53]. Research was focused primarily on lowering the melting point of Cu–Ag–Nb to make casting easier. UTS of 1840 MPa was achieved in Cu-8.2 wt%Ag-4wt%Nb wires drawn to a strain of 10.5 [14]. To analyze the reasons behind this very high strength, researchers investigated Nb dendrites, Nb filaments, and Ag–Cu or Cu–Nb interaction [51–56] but they did not include the possibility of synergistic effects between Nb and Ag with respect to CP, DP, strength and conductivity. To study synergy, Nb content would have to be sufficiently low that strengthening effects could not be attributed to Ag or Nb alone. No studies of Cu–Ag–Nb so far, however, have addressed Nb content lower than 4 wt%.

In this work, we studied the influence of Nb doping on the kinetics of Ag precipitation. We found that Nb doping had a disproportionate synergistic effect on the ratio of CPs to DPs, thus producing high strength at relatively low cost.

2. Experimental procedure and calculations

Both Cu-7.9 wt%Ag and Cu-5.8 wt%Ag-0.6 wt%Nb alloys were cast by ACI Alloys, Inc., USA. The chemistry of these alloys was measured by Energy Dispersive Spectrometer (EDS), (Table 1). The strengthening elements (Ag in the Cu–Ag alloy and Ag plus Nb in the Cu–Ag–Nb alloy) were intended to have the same weight percent, but, because of the high melting temperature of Nb, more Ag evaporated in the Cu–Ag–Nb alloy, so the Ag content in that alloy turned out to be lower than expected. We

decided to continue nonetheless because, if the Cu–Ag–Nb alloy turned out to be stronger despite a lower percentage of strengthening element (Ag + Nb), we would be able to demonstrate synergy between Ag and Nb. We sectioned as-cast ingots, treated them at 760 °C for 25 h, and quenched them in water.

Solution-treated samples were characterized during heating from 100 °C to 500 °C under an argon atmosphere in a differential scanning calorimeter (DSC: Shimadzu DSC-60). The heating rates ranged from 5 °C/min to 50 °C/min. Exothermic peaks were determined by calculating the local maximum values, which were estimated at the temperature where the derivative of dQ/dt with respect to temperature was zero (i.e. $d(dQ/dt)/dT = 0$). We arrived at the onset temperatures of precipitation reactions using the intersection points of the extrapolated baselines and inflectional tangents at the beginning of precipitation. We calculated the baseline and the inflectional tangent from the temperature-dependent heat flow signal.

The quenched ingots were also machined into several samples with dimensions of 100 mm × 15 mm × 0.5 mm and isothermally aged at 170 °C and 475 °C for times ranging from 0.5 h to 16 h. All the heat treatments were performed in an argon atmosphere. Additionally, two rectangular specimens sectioned from the two as-cast ingots (initial thickness of 5 mm) were cold rolled to a total reduction of 97.6% without any intermediate heat treatment (final thickness was about 0.12 mm). The reduction is defined as $100 \times (t_0-t)/t_0$, where t_0 is the initial specimen thickness and t is the thickness after cold rolling.

Both as-cast and heat-treated samples were electrically polished in a solution of 30% phosphoric acid and 70% water, and examined in a field emission scanning electron microscopy (FESEM, Zeiss 1540 XB). Samples for transmission electron microscopy (TEM) were prepared by grinding a 3-mm diameter disk to approximately 100 μm, and twin-jet polished in a solution of 50% nitric acid in water at −30 °C with a voltage of 8 V in a Struers TenuPol 5. The foils were observed in a JEOL-2011 TEM operating at 200 kV.

Microhardness tests were performed using a diamond indenter under a load of 0.3 kg for as-cast and heat-treated samples, and a load of 0.05 kg for as-rolled samples with a dwelling time of 10 s. The hardness of heat-treated samples was measured on the longitudinal cross-sections. The hardness of as-rolled samples was measured on the rolling plane. In order to reduce the influence of fluctuation of temperature and ions, electrical resistivity was measured by standard four-point probe method in both deionized water at room temperature and in liquid nitrogen at −196 °C. Tensile tests were carried out at room temperature using a Tytron 250 Microforce Testing System with an initial strain rate of 3 × 10^{-4} s^{-1}. The samples used for tensile tests were too small to allow strain to be measured by extensometer, so the digital image correlation (DIC) technique was used. For each experimental condition (as-cast, heat-treated, or as-rolled) at least three samples were used.

3. Results

3.1. As-cast microstructure

In all the alloys that we studied, we found degenerated Cu–Ag eutectics embedded in the Cu matrix (Fig. 1a and c). High magnification images revealed the morphology of Ag precipitates within the Cu matrix of each composite. In the Cu–Ag–Nb alloy, Nb particles were also embedded (Fig. 1b, d, and 2). A high magnification image was necessary in order to reveal the ovoid morphology of Nb (Fig. 1b inset). In the Nb-doped alloy, the lower Ag content resulted in a 3% decrease in the volume fraction of degenerated eutectics (see Table 1). Both CPs and DPs appeared in SEM images of doped and undoped alloys (Fig. 1c and d). In the un-doped alloy, the volume fraction of CP was small. We could only examine its morphology in a selected area by using high-magnification images (Fig. 1c inset). In the doped alloy, the area of Ag precipitates (including DPs and CPs) was measured by metallographic point-counting at about 2/3, compared to approximately 1/3 in the un-

Table 1
Chemical analysis of as-received alloys utilizing EDS.

	Weight fraction (%)		Calculated Volume fraction (%)	
	Ag	Nb	Ag	Nb
Cu–Ag	7.9 ± 0.6	/	8.9 ± 0.7	/
Cu–Ag–Nb	5.8 ± 0.7	0.6 ± 0.1	6.2 ± 0.8	0.6 ± 0.1
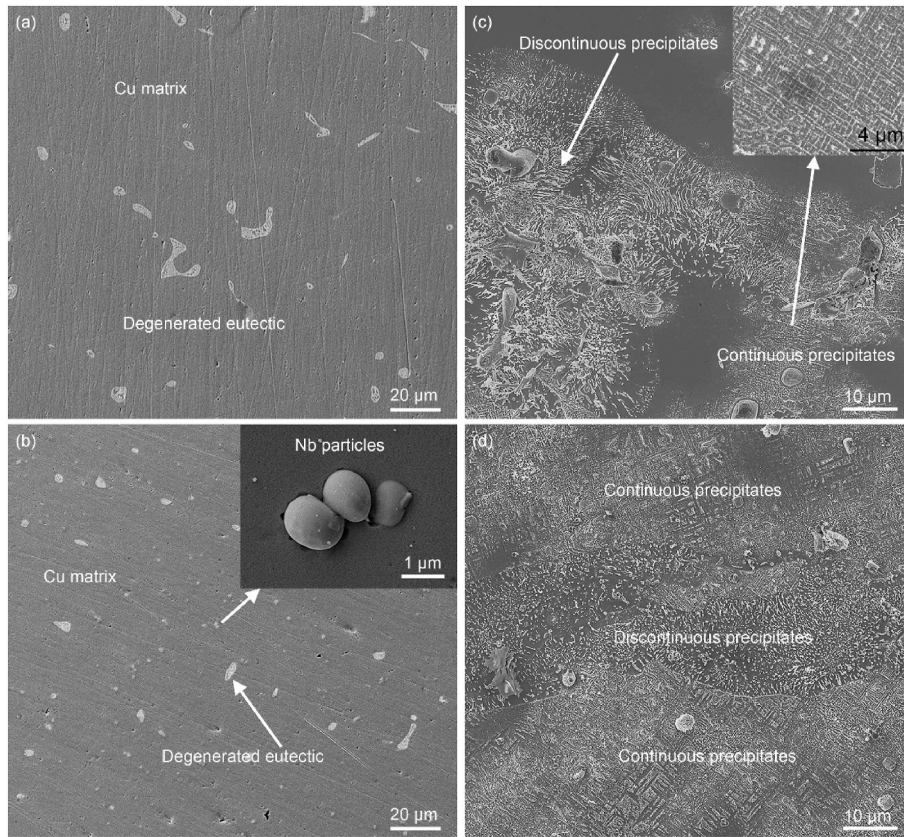
Fig. 1. As-cast microstructure of Cu–Ag (a) and Cu–Ag–Nb (b), along with their respective magnified images (c, d).

doped alloy, indicating that Nb addition increased the volume fraction of Ag precipitation. The spacing between DPs was almost same in the two alloys (approximately 400 nm), but the spacing between CPs was approximately 30 nm greater in the Nb-doped alloy (Table 2). The area percentage of CPs in the Nb-doped alloy was visibly higher than in the un-doped alloy.

Rod-like Ag precipitates appeared in both bright-field and dark-field TEM images of as-cast Cu–Ag–Nb alloy. These precipitates showed up in contrast to the surrounding field, i.e., dark contrast in the bright-field image, bright contrast in the dark-field image (Fig. 2a and b). A partial selective area diffraction pattern (SADP) revealed diffraction spots of Nb between the spots of Ag and Cu, indicating that Nb is a distinct phase (Fig. 2c). The complete SADP revealed brighter diffraction spots from Ag than from Nb, indicating a large volume fraction of Ag precipitates (Fig. 2c inset). We found a defined orientation relationship between Nb and Cu, indicating that Nb forms during the solid-state reaction. The nanoparticles were mainly from Nb in the dark-field image taken by $(110)_{Nb}$ diffraction (Fig. 2d). These very small nanoparticles were probably the result of precipitation reaction.

Our EDS results showed that Ag content in the Cu matrix of the Nb-doped alloy was lower than in the Cu–Ag alloy. The volume fraction of Nb particles in the dark-field image was 1.5%, as measured by metallographic point-counting (Fig. 2d). This value was much higher than the overall Nb content (see Table 1). This difference may have resulted from inaccurate measurement of sample thickness or from inaccurate identification of some Ag particles as Nb particles. The $(110)_{Nb}$ and $(111^-)_{Ag}$ diffraction spots from two separate phases appeared very close together in the partial SADP (Fig. 2c). Some of the bright contrast in the dark field image might be Ag precipitates rather than Nb precipitates (one of them is indicated by Nb/Ag precipitate in Fig. 2d), which would account for an artificially high volume fraction of Nb.

The solubility of bulk Nb in Cu is negligible [14]. Our EDS results in SEM, however, indicated the presence of some Nb content (0.15 vol%) in

the area of Cu matrix that did not have any visible particles, indicating the presence Nb (see Table 2). We estimated that, out of the overall volume fraction of 0.6 vol% Nb, 0.15 vol% constituted nanoparticles. We assumed that Ag accounted for 1.35 vol% of the 1.5 vol% of precipitates that appeared in our dark field images.

3.2. Precipitation behaviors of Nb-doped alloy

3.2.1. Precipitation kinetics of Ag

DSC curves of quenched Nb-doped alloy showed two exothermic peaks during heating (Fig. 3a). In samples subjected to higher heating rates, exothermic peaks shifted toward higher temperatures. These results are consistent with previous work on Cu–Ag alloy [39]. The first set of peaks, those indicating DPs of Ag, appeared between 260 °C and 370 °C, which were lower than that in un-doped alloy (300°C-400 °C). The second set of peaks, those indicating CPs of Ag, appeared above 450 °C. The onset temperature for the DP reaction was lower in Nb-doped alloy than in un-doped alloy at the same heating rate, but similar for CPs.

According to the equation developed by Kissinger:

$$\ln\left(b \left/ T_p^2\right.\right) = -E_a \left/ \left(R T_p\right)\right. + C \tag{1}$$

where b is the heating rate, T_p is the peak temperature in the DSC curve, E_a is the activation energy, R is the universal gas constant, and C is a constant. We determined exothermic peaks by calculating local maximum values, estimated at the temperature where the derivative of dQ/dt respective to temperature was zero (i.e. $d(dQ/dt)/dT = 0$). The activation energy values for DP and CP reactions were calculated according to equation (1) as 63±5 kJ/mol and 125±12 kJ/mol, respectively (Fig. 3b). Activation energy value for DPs in Cu–Ag–Nb alloy was almost the same as in Cu–Ag alloy (63.7 kJ/mol) [42]. The activation energy value for CPs, however, was significantly higher in the doped
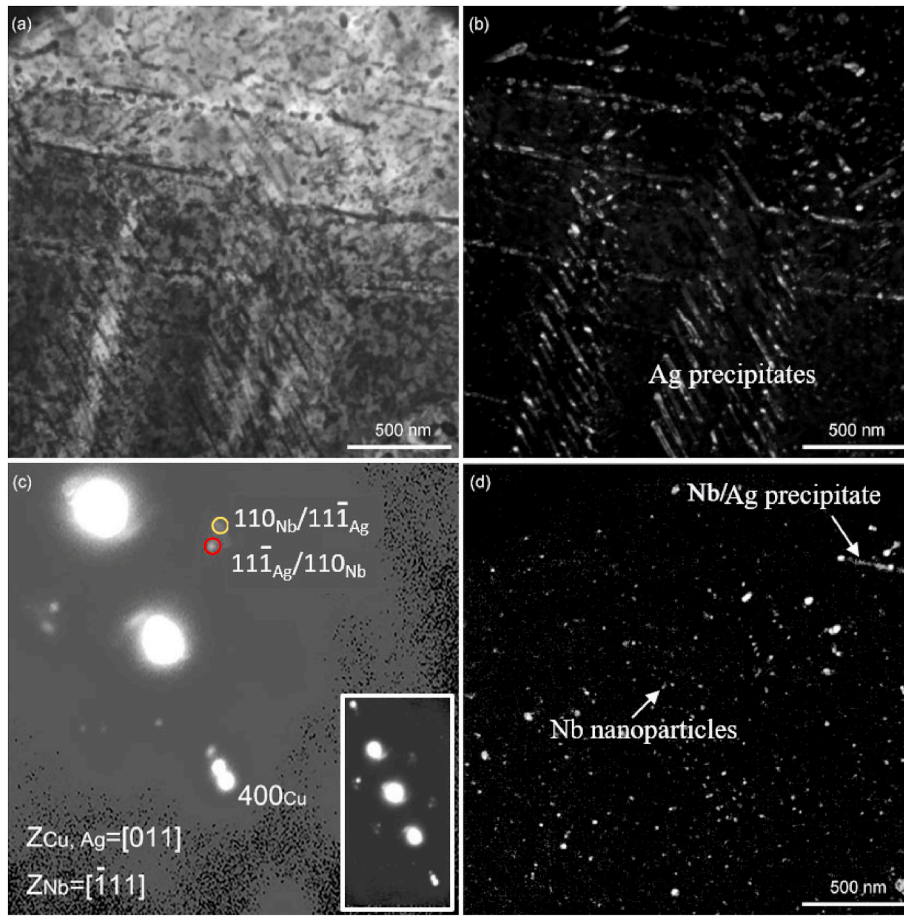
Fig. 2. TEM bright-field image (a) with corresponding SAD patterns (c) and dark field image (b, d) of an as-cast Cu–Ag–Nb alloy.

Table 2
Summary of microstructural characterizations in as-cast Cu–Ag and Cu–Ag–Nb alloys.

Description	Cu–Ag	Cu–Ag–Nb
volume fraction of degenerated eutectics	4.5%	1.5%
spacing between DPs (nm)	400 ± 20	400 ± 10
average diameter of DPs (nm)	124 ± 50	116 ± 30
spacing between CP rows (nm)	198 ± 68	228 ± 59
spacing between CPs (nm)	74 ± 17	103 ± 13
size of CPs (nm)	53 ± 6	75 ± 17
Ag content in Cu matrix from SEM-EDS (wt%)	$5.8 \pm 0.3\%$	$4.1 \pm 0.6\%$
Nb content in Cu matrix from SEM-EDS (wt%)	–	0.15%

than in the undoped alloy (68.7 kJ/mol) [39]. We speculated that this higher value might be the result of the addition of Nb to the system.

3.2.2. Microstructural evolution

We found very few Ag precipitates in solution-treated Cu–Ag–Nb alloy, indicating that Ag had almost completely dissolved in the Cu matrix (Fig. 4a). Solution treatment, however, had no influence on the morphology of the Nb particles, which remained ovoid in shape (Fig. 4b).

DSC is often used to determine the aging temperature for non-isothermal precipitation, usually 50 °C to 100 °C higher than for isothermal precipitation. For our isothermal aging temperature, we selected 170 °C, a value within the range suggested by our DSC results. At this temperature, SEM images showed spherical Ag precipitates, mostly small in diameter, in both types of samples (as indicated by white arrows in Fig. 5). In Cu–Ag samples aged isothermally at 170 °C, a small
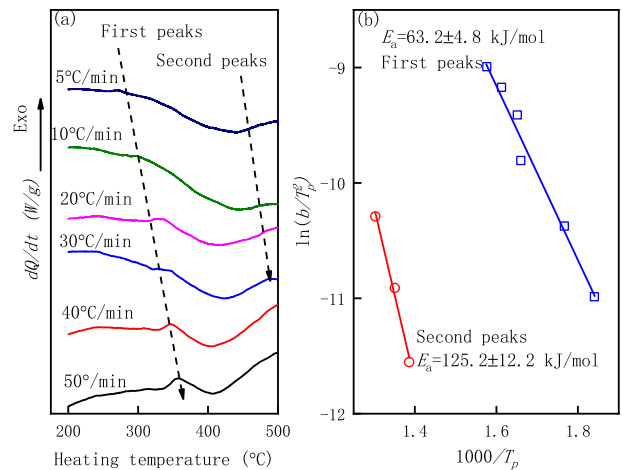
Fig. 3. DSC curves of Cu–Ag–Nb samples subjected to different heating rates (a) and Kissinger plot for calculating activation energies of two distinct exothermic reactions (b).

number of Ag precipitates appeared (Fig. 5a, b, 5c). We subjected our samples to several aging times in order to investigate the effect on precipitation reaction at 170 °C. In general, volume fraction of precipitation (Cu with Ag precipitates) was higher in doped than in undoped samples, especially after prolonged heat treatment (compare Fig. 5c to f). That said, prolonging aging time introduced almost no change in the volume fraction of Ag precipitates in undoped samples but considerable change in doped samples. Volume fraction of precipitation in doped
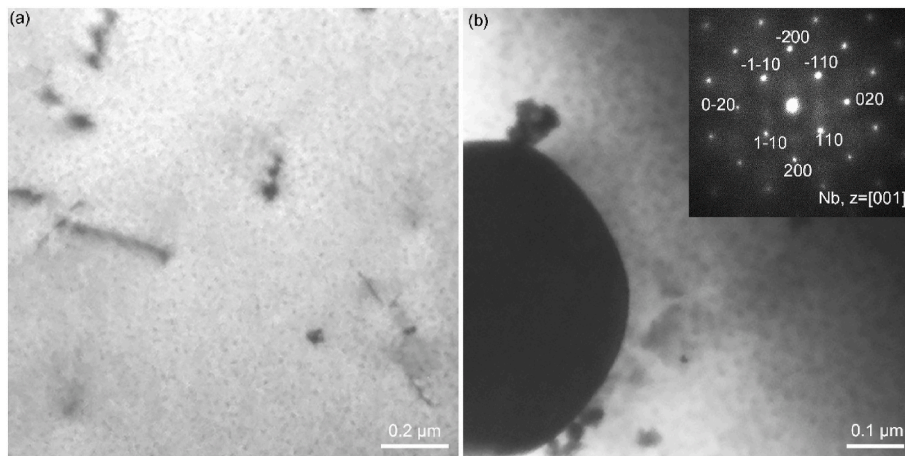
Fig. 4. (a) TEM image within Cu-matrix zone and (b) morphology of one Nb particle in quenched Cu-5.8 wt%Ag-0.6 wt%Nb alloy. The inset in (b) is the indexed SADP of the Nb particle.

samples increased about 0.76% in the sample treated for 0.5 h and 1.7% in the sample treated for 16 h. In undoped samples, however, while volume fraction of precipitation was about 0.4% in the sample treated for 0.5 h, it was only about 0.55% in the sample treated for 16 h. In doped samples, high-magnification images showed the presence of rod-shaped precipitates (see Fig. 5f inset). We speculate that precipitation reaction may have occurred at a much lower temperature in the doped samples that had been subjected to prolonged heat treatment. This is consistent with our DSC results.

For a second aging temperature, we selected 475 °C because we found that both strength and electrical conductivity reach their best values in Cu–Ag alloy at that temperature [39]. In doped samples heat-treated at 475 °C, both DPs and CPs of Ag appeared in large quantity (Fig. 6). The volume fraction of Ag precipitation was significantly higher than in samples treated at 170 °C. In the as-cast condition or during the early stages of aging, the spacing of DPs was almost identical in doped and undoped samples. In undoped samples, increasing treatment time from 0.5 h to 1 h resulted in a 35% increase in spacing. The t-test results showed significant difference, with a confidence level of 90%. Spacing in the doped sample treated for 1 h, however, was not significantly different from spacing in the sample treated for 0.5 h (Fig. 7a). This demonstrates that heat treatment time had a greater influence on the undoped samples. We also measured the average diameter of DPs in doped and undoped samples after different aging times. This diameter was larger in doped than in undoped samples treated for 0.5 h, (Fig. 7b). With increasing aging time, this diameter increased substantially in undoped samples but showed no significant change in doped samples. Consequently, this diameter was much smaller in the doped sample treated for 16 h.

3.2.3. Hardness and electrical resistivity

The hardness of aged Nb-doped samples increased as aging time increased, reaching a peak value of 120 HV after 1 h and remaining relatively high thereafter (Fig. 8a). The hardness of aged, undoped Cu–Ag samples also increased as aging time increased, but it reached a peak value of only 108 HV after 1 h and fell rapidly thereafter. After aging for 1 h, hardness values for doped samples were 16% higher; after aging for 16 h, they were 63% higher. The hardness difference between doped and undoped samples is significant with 95% confidence level, according to t-test results.

Values for electrical resistivity, as measured at 25 °C ($\rho_{25\,°C}$) and at −196 °C ($\rho_{-196\,°C}$), were almost the same for doped and undoped samples after up to 2 h of aging. After aging longer than 2 h, however, these values were somewhat higher in doped samples (Fig. 8b). For each sample, we estimated the residual resistivity ratio between readings

taken at 25 °C and at −196 °C, using the formula $\rho_{25\,°C}/\rho_{-196\,°C}$. Doped samples consistently had slightly lower ratios than undoped samples. In both cases, ratios increased significantly with increasing aging time up to 4 h, after which point additional aging time produced no significant increase.

3.3. Anisotropy in tensile properties and electrical resistivity

In deformed sheets of doped and undoped Cu–Ag, both tensile strength and electrical resistivity showed anisotropy. Ultimate tensile strength (UTS) and yield strength (YS) were approximately 3–6% higher in transverse section (TS) than in longitudinal section (LS) (see Table 3). In doped sheets, UTS was higher by 5% and YS by 6%. Nb doping had no appreciable impact on elongation, which remained greater in LS than in TS. Electrical resistivity in doped sheets was 5% higher in LS and 4% higher in TS.

4. Discussion

4.1. Influence of Nb doping on Ag precipitation

By influencing the kinetics of Ag precipitation, Nb doping enhances the mechanical strength of Cu–Ag composites. In our doped, as-cast samples, large Ag precipitates predominated, while in undoped samples, Ag precipitates remained small and few. During casting, both doped and undoped samples had been exposed to same high temperature, but the resulting precipitation was clearly greater in doped samples.

For undoped samples, high temperature aging resulted in coarsening of DPs, but when doped samples were kept at a high temperature for up to 16 h of isothermal aging, the size and spacing of DPs remained almost the same (Fig. 7).

The Ostwald coarsening equation, which could be used to describe the un-doped alloy, could not be applied to Nb-doped composite aged for 0.5 h–16 h. The discrepancy can be illustrated as follows:

$$r^3 - r_0^3 = \frac{8DC_e\gamma V_m^2}{9RT}\cdot t \qquad (2)$$

where r is the precipitate radius at time t and r_0 is the precipitate radius at time zero. D is the diffusivity of the elements, C_e is the equilibrium solubility at a given temperature, γ is the interfacial energy, V_m is the molar volume of the precipitate. Using our measured minimum Ag precipitate radius of 25 nm as r_0, $\frac{8DC_e\gamma V_m^2}{9RT}$ was estimated to be 3.8×10^4 nm^3/h. The measured data showed that Nb-doped Cu–Ag had a
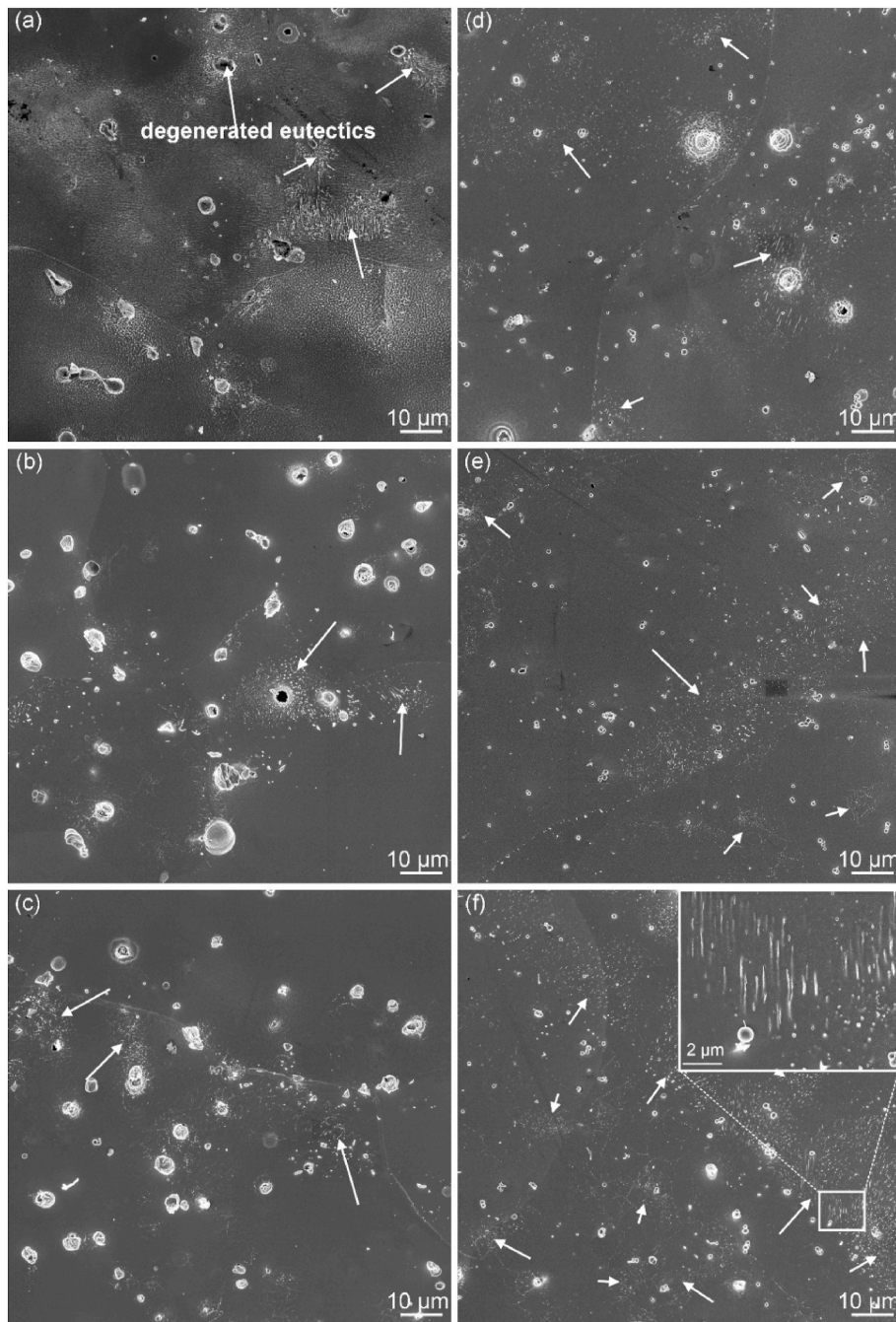
Fig. 5. Microstructures of the 170 °C -treated Cu–Ag (a, b, c) and Cu–Ag–Nb (d, e, f) alloys after different time of aging: 0.5 h (a, d), 2 h (b, e), 16 h (c, f).

surprisingly low value for $\frac{8DC_e\gamma V_m^2}{9RT}$. Furthermore, the precipitate radius in samples subjected to 16 h of isothermal heat treatment was smaller for Nb-doped Cu–Ag than for un-doped Cu–Ag. Nb may have reduced the values for D, C_e, and/or γ. Furthermore, the molar volume of Ag (V_m in Equation (2)) in Nb-doped Cu–Ag was 36% smaller than un-doped.

In samples subjected for 0.5 h to 475 °C isothermal heat treatment, the diameter of DPs was larger in Nb-doped than in un-doped Cu–Ag, indicating that Nb promotes formation or nucleation of DPs. Similar promotion by Nb of DPs nucleation occurred in samples isothermally aged at 170 °C, in which the observed volume fraction of DPs was much greater in Nb-doped than in un-doped Cu–Ag. Doping with Nb increased the volume fraction of areas with CPs more than those with DPs. This appears to indicate that Nb addition affects CPs and DPs differently. This difference can sometimes be correlated to continuous reaction

experiments.

DSC was used to undertake this research. In Cu–Ag alloys, the activation energy for CPs is slightly larger than for DPs [39]. Doping with Nb increases the activation energy of CPs. This indicates that Nb affects the kinetics of CPs more than of DPs. More work is required to correlate this to the isothermal kinetics of Ag precipitation in Nb-doped samples.

4.2. Influence of Nb doping on maintaining hardness

In our as-cast alloys, grain boundary strengthening and dislocation strengthening were negligible. Solution treatment maximized solid solution strengthening in both un-doped and doped samples. During isothermal ageing, however, the solid solution hardening effect decreased and precipitation hardening increased because the formation of both DPs and CPs reduced the solid solution present in Cu. During the
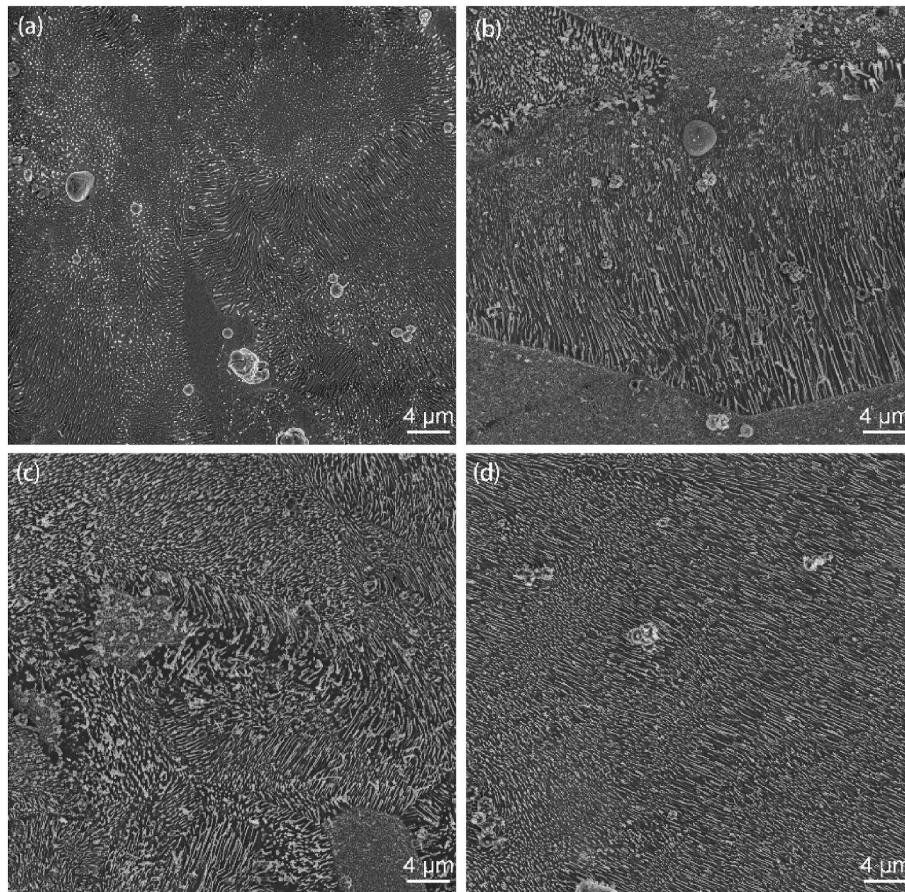
Fig. 6. Microstructure of Cu–Ag–Nb treated at 475 °C for 0.5 h (a), 1 h (b), 4 h (c), 16 h (d).
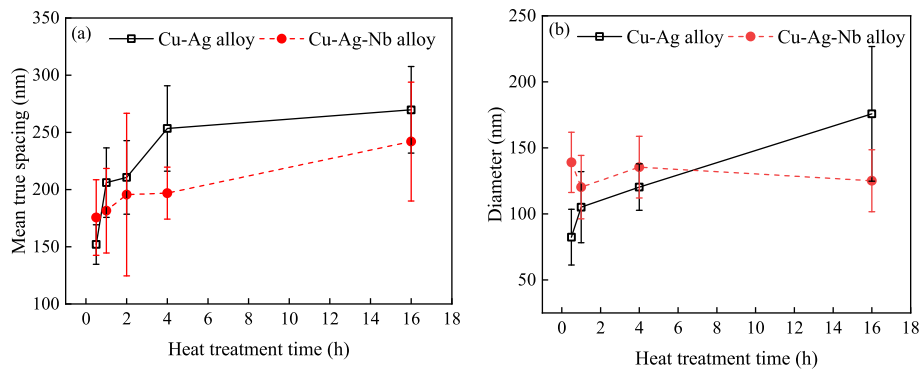
Fig. 7. Comparison of heat-treated Cu–Ag and Cu–Ag–Nb by mean true spacing (a) and diameter (b) of DPs (Cu–Ag data from previous publication [39]).

first hour of isothermal aging, because of the formation of both Ag DPs and Ag CPs, hardness increased at least 10% in un-doped and 20% in doped samples (Fig. 8). After 1 h of isothermal heat treatment, the hardness of doped samples changes little because Nb slows down the growth and coarsening of Ag DPs. Although the spacing between Ag DPs in doped samples was initially higher than in un-doped samples, it leveled off after the first hour of heat-treatment and did not increase thereafter. In un-doped samples, however, the spacing increased with increasing heat treatment time, up to as much as 16 h. Meanwhile, the precipitate spacing of CPs remained much smaller than that of DPs in both doped and un-doped samples. Any area of a sample that has greater density of Ag CP would have higher hardness. Thus, high volume fraction of CPs with fine spacing results in higher hardness in doped samples that have been treated for more than an hour. The hardness of these

samples remains at a high level after prolonged heat-treatment because of the lower coarsening rate of Ag precipitates, both CPs and DPs.

4.3. Influence of Nb doping on strengthening effect

In as-cast Cu–Ag and Cu–Ag–Nb alloys, Ag solubility in Cu was calculated from resistivity. This calculation gave 0.8 wt% for Cu–Ag and 0.7 wt% for Nb-doped Cu–Ag. Considering both solid solution strengthening and Ag precipitate strengthening, the strength values (σ_i, i = CP or DP) of Cu–Ag and Cu–Ag–Nb sheets can be calculated as follows [7]:

$$\sigma_i = \sigma_{0Cu} + k\sqrt{\frac{x_a}{3}} + k_{Cu/Ag}\lambda_0^{-1/2}exp(\varepsilon\,/\,4) \qquad (3)$$
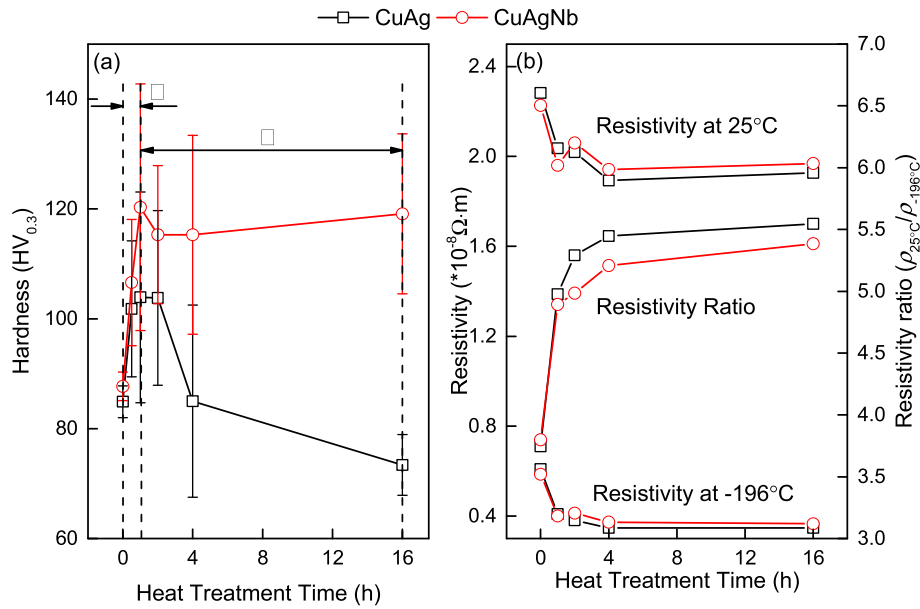
Fig. 8. Hardness and resistivity in 475°C-treated Cu–Ag and Cu–Ag–Nb. Fig. 8a: Hardness as a function of heat treatment time. Zone I indicates the stage of nucleation and growth of Ag precipitates. Zone II indicates the stage of growth and coarsening of Ag precipitates. Fig. 8b: Resistivity and residual resistivity ratio ($\rho_{25°C}/\rho_{-196°C}$) as a function of heat treatment time.

Table 3
Summary of properties in Cu–Ag and Cu–Ag–Nb samples.

Direction	As-rolled Cu–Ag alloy		As-rolled Cu–Ag–Nb alloy	
	Longitudinal	Short Transverse	Longitudinal	Short Transverse
Resistivity (nΩm)	23.0	22.7	24.1	23.6
Yield strength (MPa)	663 ± 10	683 ± 4	704 ± 4	723 ± 3
UTS (MPa)	704 ± 9	738 ± 17	741 ± 6	788 ± 6
Elong.%	4.7 ± 0.7	3.2 ± 0.3	4.1 ± 0.7	3.2 ± 0.2

where σ_{0Cu} is the intrinsic friction stress of pure Cu, k is a function of the alloying element and the lattice parameter change due to element addition, x_a is the atomic fraction of Ag dissolved in Cu, $k_{Cu/Ag}$ is the strengthening coefficient for proeutectic Cu/Ag, λ_0 is the initial scale of the Ag precipitates in Cu matrix, ε is the deformation strain. Using the same method as in our previous work [35], k was calculated as 0.0267 for Cu–Ag and 0.0233 for Nb-doped Cu–Ag. The value for $k_{Cu/Ag}$ was estimated to be 0.11 MPa$\sqrt{m}$ [30]. The value for ε was 3.7 for our Cu–Ag sheets. Both CPs and DPs were observed in as-cast Nb-doped and un-doped Cu–Ag. Because of a difference in both size and spacing (Table 2), contributions from DPs and CPs were considered separately (σ_{DP} and σ_{CP} in Table 4). Our calculation results showed that the precipitation strengthening of Ag precipitates played an important role in

Table 4
Individual contributions to the total strength of Cu–Ag and Cu–Ag–Nb sheets with a deformation strain of 3.7.

σ_{Cu} (MPa)	Cu–Ag sheet		Cu–Ag–Nb sheet	
	33		33	
Ag solid solution hardening (MPa)	**103**		**96**	
Ag precipitate hardening (MPa)	DPs	CPs	DPs	CPs
	450	752	450	681
Strength (σ_{DP} or σ_{CP}, MPa)	586	888	579	810
Yield strength (measured, MPa)	Longitudinal	Transverse	Longitudinal	Transverse
	663 ± 10	683 ± 4	704 ± 4	723 ± 3

the overall strength, which was consistent with previous work [30]. Strengthening by CPs is much higher than by DPs because of smaller spacing (Table 4). The measured yield strength values of un-doped and Nb-doped Cu–Ag sheets were both in range of σ_{DP} and σ_{CP}. The higher percentage of CPs in as-cast Cu–Ag–Nb is responsible for the higher strength of Cu–Ag–Nb sheet.

On the other hand, it is widely recognized that the storage of dislocations in the interface can contribute to material strengthening [57]. In Cu–Ag–Nb sheet, the Nb particle was also deformed during the rolling, and formed an interface between Cu and Nb. It has been proved that the interfaces of Cu/Nb play an important role for dislocation pile-ups as the grain boundaries in traditional bulk materials in Cu–Nb multilayer composite. As a result, the interfaces of Cu/Nb in as-rolled Cu–Ag–Nb alloy might also responsible for the higher strength.

5. Conclusions

(1) Adding Nb to Cu–Ag not only strengthened the Cu matrix, but also enhanced the strengthening effect of Ag precipitates by a disproportionate synergistic effect on the ratio of CPs to DPs.
(2) Both nano-sized Nb precipitates and spherical Nb particles (with an average diameter of 0.9 μm) were found in the Cu matrix of as-cast Nb-doped Cu–Ag.
(3) The activation energy of CPs of Ag was higher in Nb-doped than in un-doped Cu–Ag. The activation energy value for the phase transition of DPs was lower than that of CPs in Nb-doped Cu–Ag.
(4) In samples subjected to high ageing temperature (475 °C), the spacing of DPs in Nb-doped Cu–Ag was smaller than that of DPs in un-doped Cu–Ag. We attributed this not only to the presence of Nb but also to the lower initial Ag content in the doped samples.
(5) The strength of as-rolled Cu–Ag composites was significantly increased not only by the presence Cu/Nb interfaces but also by a higher volume fraction of CPs.
(6) Electrical conductivity in Cu–Ag was only marginally decreased by Nb-doping.

CRediT authorship contribution statement

Congcong Zhao: Conceptualization, Writing - original draft, Formal

analysis, Writing - review & editing, conceived and designed the experiments, performed the experiments, analyzed the data, wrote the draft, All authors reviewed the manuscript. **Rongmei Niu:** Writing - original draft, Writing - review & editing, performed the experiments, revised the draft, All authors reviewed the manuscript. **Yan Xin:** Writing - original draft, Formal analysis, Writing - review & editing, contributed the TEM operation and analysis, revised the draft, All authors reviewed the manuscript. **Daniel Brown:** Writing - original draft, Writing - review & editing, contributed to the heat treatments and electrical resistivity tests, respectively, revised the draft, All authors reviewed the manuscript. **David McGuire:** Writing - review & editing, contributed to the heat treatments and electrical resistivity tests, respectively, All authors reviewed the manuscript. **Engang Wang:** Conceptualization, Supervision, Writing - review & editing, conceived and designed the experiments, co-supervised the project, All authors reviewed the manuscript. **Ke Han:** Conceptualization, Writing - original draft, Formal analysis, Supervision, Writing - review & editing, conceived and designed the experiments, analyzed the data, co-supervised the project, revised the draft, All authors reviewed the manuscript.

Declaration of competing interest

On behalf of all the authors, we disclose that we have no interests that might appear to affect our ability to present data objectively. These include relevant financial (for example patent ownership, stock ownership, consultancies, speaker's fees), personal, political, intellectual, or religious interests.

Acknowledgments

Data availability statement

All data included in this study are available upon request by contact with the corresponding authors.

Appendix A. Supplementary data

Supplementary data to this article can be found online at https://doi.org/10.1016/j.msea.2020.140091.

References

[1] National Reaearch Council, High Magnetic Field Science and its Application in the United States: Current Status and Future Directions, National Academies Press, Washington, DC, 2013.

[2] U. Hangen, D. Raabe, Modeling of the yield strength of a heavily wire drawn Cu-20%Nb composite by use of a modified linear rule of mixtures, Acta Metall. Mater. 43 (1995) 4075–4082, https://doi.org/10.1016/0956-7151(95)00079-B.

[3] S. Foner, 68.4-T-long pulse magnet: test of high strength microcomposite Cu/Nb conductor, Appl. Phys. Lett. 49 (1986) 982, https://doi.org/10.1063/1.97503.

[4] L. Deng, K. Han, K.T. Hartwig, T.M. Siegrist, L. Dong, Z. Sun, X. Yang, Q. Liu, Hardness, electrical resistivity, and modeling of in situ Cu-Nb microcomposites, J. Alloys Compd. 602 (2014) 331–338, https://doi.org/10.1016/j.jallcom.2014.03.021.

[5] V.I. Pantsyrnyi, A.K. Shikov, A.D. Nikulin, A.E. Vorob'ova, E.A. Dergunova, A.G. Silaev, N.A. Bel'akov, I.I. Potapenko, Development of Cu-Nb alloy microcomposite conductors for high field pulsed magnets, IEEE Trans. Magn. 32 (1996) 2866–2869, https://doi.org/10.1109/20.511473.

[6] L. Deng, X. Yang, K. Han, Y. Lu, M. Liang, Q. Liu, Microstructure and texture evolution of Cu-Nb composite wires, Mater. Char. 81 (2013) 124–133, https://doi.org/10.1016/j.matchar.2013.04.013.

[7] K. Han, J.D. Embury, J.R. Sims, L.J. Campbell, H.J. Schneider-Muntau, V.I. Pantsyrnyi, A. Shikov, A. Nikulin, A. Vorobieva, The fabrication, properties and microstructure of Cu-Ag and Cu-Nb composite conductors, Mater. Sci. Eng., A 267 (1999) 99–114, https://doi.org/10.1016/S0921-5093(99)00025-8.

[8] Y.L. Wang, K. Han, Y. Huang, K.Y. Zhang, Microstructure in Cu-Nb microcomposites, Mater. Sci. Eng. 351 (2003) 214–223, https://doi.org/10.1016/s0921-5093(02)00855-9.

[9] D. Raabe, U. Hangen, Correlation of microstructure and type II superconductivity of a heavily cold rolled Cu-20mass% Nb in situ composite, Acta Mater. 44 (1996) 953–961, https://doi.org/10.1016/1359-6454(95)00239-1.

[10] F. Heringhaus, D. Raabe, G. Gottstein, On the correlation of microstructure and electromagnetic properties of heavily cold worked Cu-20 wt% Nb wires, Acta Metall. Mater. 43 (1995) 1467–1476, https://doi.org/10.1016/0956-7151(94)00378-U.

[11] D. Raabe, U. Hangen, Observation of amorphous areas in a heavily cold rolled Cu-20 wt% Nb composite, Mater. Lett. 22 (1995) 155–161, https://doi.org/10.1016/0167-577X(94)00248-7.

[12] W.A. Spitzig, P.D. Krotz, A comparison of the strength and microstructure of heavily cold worked Cu-20% Nb composites formed by different melting procedures, Scripta Metall. 21 (1987) 1143–1146, https://doi.org/10.1016/0036-9748(87)90266-3.

[13] W.A. Spitzig, A.R. Pelton, F.C. Laabs, Characterization of the strength and microstructure of heavily cold worked Cu-Nb composites, Acta Metall. 35 (1987) 2427–2442, https://doi.org/10.1016/0001-6160(87)90140-4.

[14] D. Raabe, F. Heringhaus, Correlation of superconductivity and microstructure in an in-situ formed Cu-20%Nb composite, Phys. Status Solidi A 142 (1994) 473–481, https://doi.org/10.1002/pssa.2211420221.

[15] A.B. Rozhnov, V.I. Pantsyrny, A.V. Kraynev, S.O. Rogachev, S.A. Nikulin, N.E. Khlebova, M.V. Polikarpova, M.Y. Zadorozhnyy, Low-cycle bending fatigue and electrical conductivity of high-strength Cu/Nb nanocomposite wires, Int. J. Fatig. 128 (2019) 105188, https://doi.org/10.1016/j.ijfatigue.2019.105188.

[16] T. Gu, O. Castelnau, S. Forest, E. Hervé-Luanco, F. Lecouturier, H. Proudhon, L. Thilly, Multiscale modeling of the elastic behavior of architectured and nanostructured Cu-Nb composite wires, Int. J. Solid Struct. 121 (2017) 148–162, https://doi.org/10.1016/j.ijsolstr.2017.05.022.

[17] C. Ding, J. Xu, X. Li, D. Shan, B. Guo, T.G. Langdon, Microstructural evolution and mechanical behavior of Cu/Nb multilayer composites processed by accumulative roll bonding, Adv. Eng. Mater. 22 (1) (2020) 1900702, https://doi.org/10.1002/adem.201900702.

[18] J.B. Liu, L. Zhang, Y.W. Zeng, L. Meng, Co-deformation in Cu-6 wt.% Ag nanocomposites, Scripta Metall. 64 (2011) 665–668, https://doi.org/10.1016/j.scriptamat.2010.12.015.

[19] Y.Z. Tian, S.D. Wu, Z.F. Zhang, R.B. Figueiredo, N. Gao, T.G. Langdon, Comparison of microstructures and mechanical properties of a Cu-Ag alloy processed using different severe plastic deformation modes, Mater. Sci. Eng., A 528 (2011) 4331–4336, https://doi.org/10.1016/j.msea.2011.01.057.

[20] T. Asano, Y. Sakai, M. Oshikiri, K. Inoue, H. Maeda, G. Heremans, L. van Bockstal, L. Li, F. Herlach, Cu-Ag wire pulsed magnets with and without internal reinforcements, IEEE Trans. Magn. 30 (1994) 2106–2109, https://doi.org/10.1109/20.305685.

[21] T. Hirota, A. Imai, T. Kumano, M. Ichihara, Y. Sakai, K. Inoue, H. Maeda, Development of Cu-Ag alloys conductor for high field magnet, IEEE Trans. Magn. 30 (1994) 1891–1894, https://doi.org/10.1109/20.305631.

[22] Y. Sakai, K. Inoue, T. Asano, H. Wada, H. Maeda, Development of high-strength, high-conductivity Cu-Ag alloys for high-field pulsed magnet use, Appl. Phys. Lett. 59 (1991) 2965–2967, https://doi.org/10.1063/1.105813.

[23] J. He, V. Ji, L. Meng, Effects of strain and annealing on the intensity and distribution of crystal texture in Cu-12 wt.% Ag, Mater. Sci. Eng., A 478 (2008) 305–313, https://doi.org/10.1016/j.msea.2007.07.051.

[24] C.A. Davy, K. Han, P.N. Kalu, S.T. Bole, Examinations of Cu-Ag composite conductors in sheet forms, IEEE Trans. Appl. Supercond. 18 (2008) 560–563, https://doi.org/10.1109/TASC.2008.922510.

[25] J. Freudenberger, H.J. Klauß, K. Heinze, A. Gaganov, M. Schaper, L. Schultz, Fatigue of highly strengthened Cu-Ag alloys, Int. J. Fatig. 30 (2008) 437–443, https://doi.org/10.1016/j.ijfatigue.2007.04.009.

[26] S.I. Hong, M.A. Hill, Mechanical stability and electrical conductivity of Cu-Ag filamentary microcomposites, Mater. Sci. Eng. 264 (1999) 151–158, https://doi.org/10.1016/S0921-5093(98)01097-1.

[27] X.W. Zuo, C.C. Zhao, R. Niu, E.G. Wang, K. Han, Microstructural dependence of magnetoresistance in CuAg alloy solidified with high magnetic field, J. Mater. Process. Technol. 224 (2015) 208–212, https://doi.org/10.1016/j.jmatprotec.2015.05.006.

[28] Y.Z. Tian, S.D. Wu, Z.F. Zhang, R.B. Figueiredo, N. Gao, T.G. Langdon, Microstructural evolution and mechanical properties of a two-phase Cu-Ag alloy processed by high-pressure torsion to ultrahigh strains, Acta Mater. 59 (2011) 2783–2796, https://doi.org/10.1016/j.actamat.2011.01.017.

[29] X.W. Zuo, R. Guo, C.C. Zhao, L. Zhang, E.G. Wang, K. Han, Microstructure and properties of Cu-6wt%Ag composite thermomechanical-processed after directionally solidifying with magnetic field, J. Alloys Compd. 676 (2016) 46–53, https://doi.org/10.1016/j.jallcom.2016.03.127.

[30] X.W. Zuo, K. Han, C.C. Zhao, R.M. Niu, E.G. Wang, Microstructure and properties of nanostructured Cu28 wt%Ag microcomposite deformed after solidifying under a

high magnetic field, Mater. Sci. Eng. 619 (2014) 319–327, https://doi.org/10.1016/j.msea.2014.09.070.

[31] A. Benghalem, D.G. Morris, Microstructure and strength of wire-drawn Cu-Ag filamentary composites, Acta Mater. 45 (1997) 397–406, https://doi.org/10.1016/S1359-6454(96)00152-8.

[32] S.I. Hong, M.A. Hill, Microstructural stability and mechanical response of Cu-Ag microcomposite wires, Acta Mater. 46 (1998) 4111–4122, https://doi.org/10.1016/S1359-6454(98)00106-2.

[33] D. Hamana, M. Hachouf, L. Boumaza, Z.E.A. Biskri, Precipitation kinetics and mechanism in Cu-7 wt% Ag alloy, Mater. Sci. Appl. 2 (2011) 899–910, https://doi.org/10.4236/msa.2011.27120.

[34] R. Monzen, K. Murase, H. Nagayoshi, C. Watanabe, Discontinuous precipitation in {100} planes in a Cu-5.7 wt% Ag alloy single crystal, Phil. Mag. Lett. 84 (2004) 349–358, https://doi.org/10.1080/09500830410001728327.

[35] J. Lin, L. Meng, Effect of aging treatment on microstructure and mechanical properties of Cu-Ag alloys, J. Alloys Compd. 454 (2008) 150–155, https://doi.org/10.1016/j.jallcom.2006.12.073.

[36] A. Gaganov, J. Freudenberger, E. Botcharova, L. Schultz, Effect of Zr additions on the microstructure, and the mechanical and electrical properties of Cu-7 wt.%Ag alloys, Mater. Sci. Eng. 437 (2006) 313–322, https://doi.org/10.1016/j.msea.2006.07.121.

[37] J. Freudenberger, N. Kozlova, A. Gaganov, L. Schultz, H. Witte, H. Jones, Magnetoresistance up to 50 T of highly strengthened Cu-Ag conductors for pulsed high field magnets, Cryogenics 46 (2006) 724–729, https://doi.org/10.1016/j.cryogenics.2006.06.002.

[38] D.W. Yao, L.N. Song, A.P. Dong, L.T. Wang, L. Zhang, L. Meng, The role of Ag precipitates in Cu-12 wt% Ag, Mater. Sci. Eng. 558 (2012) 607–610, https://doi.org/10.1016/j.msea.2012.08.060.

[39] C.C. Zhao, X.W. Zuo, E.G. Wang, R.M. Niu, K. Han, Simultaneously increasing strength and electrical conductivity in nanostructured Cu-Ag composite, Mater. Sci. Eng. 652 (2016) 296–304, https://doi.org/10.1016/j.msea.2015.11.067.

[40] K.N. Braszczyńska-Malik, Discontinuous and continuous precipitation in magnesium-aluminium type alloys, J. Alloys Compd. 477 (2009) 870–876, https://doi.org/10.1016/j.jallcom.2008.11.008.

[41] S. Dodla, P. Thiem, M. Krüger, D. Dietrich, A. Bertram, Microstructure, flow behavior, and bulk texture evolution of cold drawn copper-silver composites, J. Alloys Compd. 647 (2015) 519–527, https://doi.org/10.1016/j.jallcom.2015.06.145.

[42] F. Dupouy, E. Snoeck, M.J. Casanove, C. Roucau, J.P. Peyrade, S. Askenazy, Microstructural characterization of high strength and high conductivity nanocomposite wires, Scripta Mater. 34 (1996) 1067–1073, https://doi.org/10.1016/1359-6462(95)00632-X.

[43] K. Han, V.J. Toplosky, R. Goddard, J. Lu, R.M. Niu, J.P. Chen, Impacts of heat treatment on properties and microstructure of Cu16at%Ag conductors, IEEE Trans. Appl. Supercond. 22 (2012) 6900204, https://doi.org/10.1109/TASC.2011.2174575.

[44] J.B. Liu, L. Zhang, A.P. Dong, L.T. Wang, Y.W. Zeng, L. Meng, Effects of Cr and Zr additions on the microstructure and properties of Cu-6 wt.% Ag alloys, Mater. Sci. Eng. 532 (2012) 331–338, https://doi.org/10.1016/j.msea.2011.10.099.

[45] H. Li, J. Jie, H. Chen, P. Zhang, T. Wang, T. Li, Effect of rotating magnetic field on the microstructure and properties of Cu-Ag-Zr alloy, Mater. Sci. Eng. 624 (2015) 140–147, https://doi.org/10.1016/j.msea.2014.11.064.

[46] J. Lyubimova, J. Freudenberger, C. Mickel, T. Thersleff, A. Kauffmann, L. Schultz, Microstructural inhomogeneities in Cu-Ag-Zr alloys due to heavy plastic deformation, Mater. Sci. Eng. 527 (2010) 606–613, https://doi.org/10.1016/j.msea.2009.08.036.

[47] W. Piyawit, W.Z. Xu, S.N. Mathaudhu, J. Freudenberger, J.M. Rigsbee, Y.T. Zhu, Nucleation and growth mechanism of Ag precipitates in a CuAgZr alloy, Mater. Sci. Eng. 610 (2014) 85–90, https://doi.org/10.1016/j.msea.2014.05.023.

[48] Y.Z. Tian, J. Freudenberger, R. Pippan, Z.F. Zhang, Formation of nanostructure and abnormal annealing behavior of a Cu-Ag-Zr alloy processed by high-pressuretorsion, Mater. Sci. Eng. 568 (2013) 184–194, https://doi.org/10.1016/j.msea.2012.11.048.

[49] F. Bittner, S. Yin, A. Kauffmann, J. Freudenberger, H. Klauß, G. Korpala, R. Kawalla, W. Schillinger, L. Schultz, Dynamic recrystallisation and precipitation behaviour of high strength and highly conducting Cu-Ag-Zr-alloys, Mater. Sci. Eng. 597 (2014) 139–147, https://doi.org/10.1016/j.msea.2013.12.051.

[50] X.C. He, H. Wang, H.S. Liu, Z.P. Jin, Thermodynamic description of the Cu-Ag-Zr system, Calphad 30 (2006) 367–374, https://doi.org/10.1016/j.calphad.2006.09.001.

[51] D. Raabe, D. Mattissen, Microstructure and mechanical properties of a cast and wire-drawn ternary Cu-Ag-Nb in situ composite, Acta Mater. 46 (1998) 5973–5984, https://doi.org/10.1016/S1359-6454(98)00218-3.

[52] D. Raabe, D. Mattissen, Experimental investigation and Ginzburg–Landau modeling of the microstructure dependence of superconductivity in Cu-Ag-Nb wires, Acta Mater. 47 (1999) 769–777, https://doi.org/10.1016/S1359-6454(98)00406-6.

[53] D. Mattissen, D. Raabe, F. Heringhaus, Experimental investigation and modeling of the influence of microstructure on the resistive conductivity of a Cu-Ag-Nb in situ composite, Acta Mater. 47 (1999) 1627–1634, https://doi.org/10.1016/S1359-6454(99)00026-9.

[54] M. Komarasamy, R.S. Mishra, S. Mukherjee, M.L. Young, Friction stir-processed thermally stable immiscible nanostructured alloys, JOM 67 (12) (2015) 2820–2827, https://doi.org/10.1007/s11837-015-1641-z.

[55] M. Komarasamy, R. Tharp, S. Sinha, S. Thapliyal, R. Mishra, Achieving forced mixing in Cu-based immiscible alloys via friction stir processing, In: Hovanski Y., Mishra R., Sato Y., Upadhyay P., Yan D. (eds) Friction Stir Welding and Processing X. The Minerals, Metals & Materials Series. Springer, Cham. https://doi.org/10.1007/978-3-030-05752-7_19.

[56] M. Palombo, A. Malagoli, M. Pani, C. Bernini, P. Manfrinetti, A. Palenzona, M. Putti, Exploring the feasibility of Fe(Se,Te) conductors by ex-situ powder-in-tube method, J. Appl. Phys. 117 (2015) 213903. https://arxiv.org/pdf/1506.01630.

[57] X. Zhang, N. Hansen, Y. Gao, X. Huang, Hall–Petch and dislocation strengthening in graded nanostructured steel, Acta Mater. 60 (16) (2012) 5933–5943, https://doi.org/10.1016/j.actamat.2012.07.037.